ACS APPLIED NANO MATERIALS

www.acsanm.org Article

Pd Nanoclusters Confined in ZIF-8 Matrixes for Fluorescent Detection of Glucose and Cholesterol

Ying Li,* Shujuan Li, Min Bao, Linqun Zhang, Carlo Carraro, Roya Maboudian, Anran Liu, Wei Wei, Yuanjian Zhang, and Songqin Liu

Cite This: *ACS Appl. Nano Mater.* 2021, 4, 9132−9142 Read Online

ACCESS | Metrics & More | Article Recommendations | Supporting Information

ABSTRACT: Nanomaterials possessing intrinsic enzyme-mimetic activity are becoming an important topic of current research. However, their enzyme-mimetic activity is limited by the particle size of the nanomaterials. In this study, Pd nanoclusters with an average size of 1.4 nm are synthesized by using a metal organic framework, zeolitic imidazolate framework-8 (ZIF-8), as a matrix via an impregnation-reaction method. By virtue of the confined channels of ZIF-8 and the strong chemical interaction between the Pd nanoclusters and ZIF-8 framework, the Pd nanoclusters show a high dispersity and stability. The obtained Pd@ZIF-8 is proven to have enhanced intrinsic peroxidase-like activity, showing Michaelis−Menten constants (K_m) as high as 0.13 mM for 3,3′,5,5′-tetramethylbenzidine and 14.02 mM for hydrogen peroxide. Colorimetric testing and electron spin resonance spectra reveal that radicals are generated during the catalytic process of peroxidase-like Pd@ZIF-8 toward H_2O_2. With the addition of glucose or cholesterol oxidase, the Pd@ZIF-8 can be utilized to construct a highly selective and sensitive fluorescent sensor for glucose and cholesterol, exhibiting a detection limit of 0.10 and 0.092 μM, respectively. Additionally, the proposed fluorescent platform exhibits the capability to detect glucose and cholesterol in serum samples with satisfactory recovery, indicating potential application prospects in biochemical analysis.

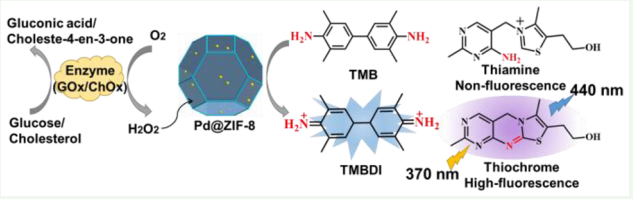

KEYWORDS: *Pd nanocluster, zeolitic imidazolate framework-8, horseradish peroxidase mimetics, cascade reaction, fluorescent detection*

1. INTRODUCTION

Hydrogen peroxide (H_2O_2) is a byproduct generated in the processing of numerous metabolites (such as glucose, cholesterol, and xanthine) which are catalytically oxidized by their corresponding oxidases, associated with oxygen consumption.[1,2] The bioproduced H_2O_2 relies on the metabolite concentrations. Therefore, the determination of in situ generated H_2O_2 is significant for the quantitative detection of the metabolite level, which plays a critical role in diagnosis and therapy. When catalyzed by peroxidases, hydrogen peroxide generates highly reactive oxygen species (ROS), such as hydroxyl radical (·OH), superoxide radical ($O_2^{\cdot-}$), and singlet oxygen ($^1O_2$).[3] These radicals with strong oxidative ability can oxidize various kinds of organic compounds, including colorless 3,3′,5,5′-tetramethylbenzidine (TMB) and thiamine, which are converted to blue 3,3′,5,5′-tetramethylbenzodiimine (TMBDI) and fluorescent thiochrome, respectively.[4,5] Based on the color or fluorescence conversion of the products, the quantity of H_2O_2 can be determined.

Horseradish peroxidase (HRP), a specific class of peroxidases, has been efficiently applied to construct a colorimetric or fluorescent platform for H_2O_2 determination due to its high catalytic activity and specificity.[6] However, as a protein, HRP has some inherent drawbacks, such as laborious preparation, easy denaturation, and difficulty in recycling, which restrict its practical applications.[7,8] Therefore, there is an urgent need to explore nanomaterial-based enzyme-mimics for the replacement of the natural enzyme. Since Fe_3O_4 magnetic nanoparticles were discovered with intrinsic peroxidase-like performance in 2007,[9,10] various enzyme-like nanomaterials have been successfully synthesized,[11−13] such as carbon nanomaterials (e.g., graphene quantum dots, carbon dots, and carbon nitrides),[5,14,15] metal oxide nanomaterials (e.g., Fe_3O_4, Co_3O_4, and CeO_2),[9,16,17] and noble metals (e.g., Au, Pt, Pd, and Ag).[18−22] In particular, noble-metal-based nanozymes are attracting extensive attention due to their activity (comparable to nature peroxidase), fascinating biocompatibility, and inherent stability.[23,24] Among them, Pd nanoparticles (NPs) with unique electronic properties and high catalytic activity are considered as a promising peroxidase-like nanozyme in biosensors fabrication.[25−29] However, the peroxidase-like activity of metal NPs is dependent on their size.[30] The metal NPs with subnanometer-scale sizes (<2 nm)

Received: June 28, 2021
Accepted: August 10, 2021
Published: August 20, 2021

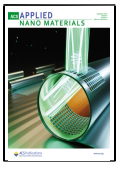

Scheme 1. Schematic Illustration of the Synthesis of Pd@ZIF-8 (Top Row) and Its Peroxidase-like Activity for the Detection of H_2O_2, Cholesterol, and Glucose (Bottom Row)[a]

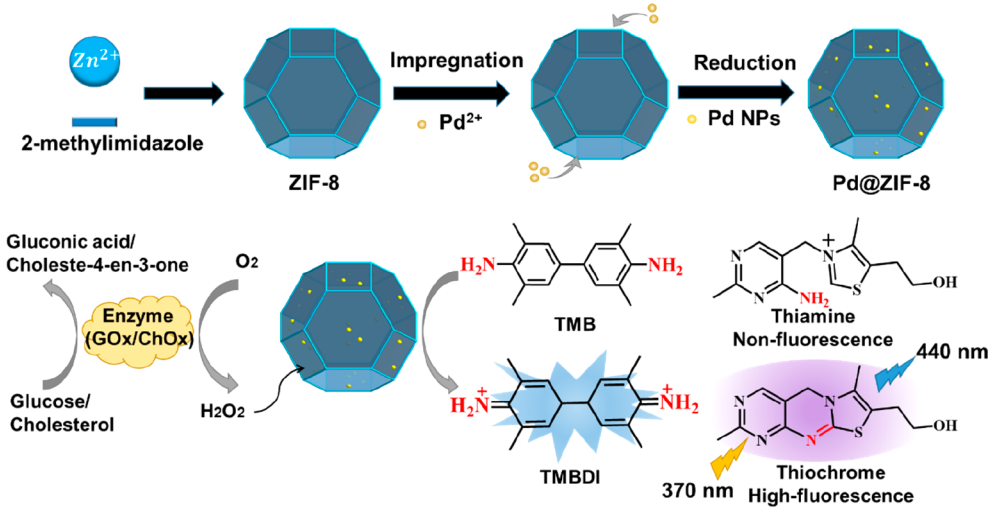

[a]Corresponding reactions are presented in Reactions 1−3.

are endowed with great catalytic efficiency and substrate specificity. Nevertheless, the noble metal NPs with subnanometer sizes are disposed toward spontaneous aggregation because of their high surface energy, which challenges their preparation and structure regulation and thereby severely limits their application.[31−33] In order to address these deficiencies, various strategies have been investigated. Li et al. synthesized 4.8 nm Pd NPs by using cytosine-rich oligonucleotides as a stabilizer, showing a K_m of 91.29 mM toward H_2O_2 and 0.03 mM toward TMB.[24] However, the functional groups of the stabilizers are prone to bioconjugation with some interferents, resulting in a relatively low exposure of active centers and thereby jeopardizing the catalytic efficiency of nanozymes.[34−36] Nowadays, immobilizing Pd NPs on carriers, such as zeolites,[37] silica,[38] carbon materials,[39−41] and metal organic frameworks (MOFs),[42−44] is an effective method to prevent Pd NPs from agglomeration.

Among them, zeolitic imidazolate framework (ZIF-8), a subclass of MOFs assembled by zinc ions and 2-methylimidazole ligands, exhibits promising properties, including the shielding effect (i.e., exceptional stability in organic and aqueous solvents and high temperature), facile synthesis under ambient conditions, high porosity and pore volume, and sufficient nitrogen-containing sites for guest anchoring.[30,45−49] Moreover, ZIF-8 does not exhibit any background interference, which is beneficial to the colorimetric and fluorescent sensing of H_2O_2. Furthermore, Lyu et al. have demonstrated that ZIF-8 offers an ideal microenvironment for the substrate accumulation through absorption for efficient enzyme catalytic reaction due to its high surface area and pore volume.[50] All these properties indicate that ZIF-8 is a promising candidate, in which highly dispersed nanometer-sized metal nanoparticles can be confined. Although much attention has been focused on preparing Pd NPs encapsulated in ZIF-8 (Pd/ZIF-8), there are only a few reports concerning their applications in peroxidase-like catalytic reactions,[51−54] not to mention toward a better understanding of their complicated catalytic pathways in H_2O_2 decomposition, which is of vital importance for their potential applications in sensing.

Herein, through a simple impregnation-reaction method, Pd nanoclusters with the size of 1.4 nm were synthesized within the cavities of the ZIF-8 matrix. Due to the high dispersity of the Pd nanoclusters and the substrate accumulation effect of ZIF-8, the as-prepared Pd@ZIF-8 displayed a highly efficient HRP-like catalysis. In the catalytic process of the Pd@ZIF-8 toward H_2O_2, radicals were produced via a Fenton-like path. Its steady-state kinetics were studied by a colorimetric method with TMB as the chromogenic substrate. The K_m of Pd@ZIF-8 with TMB as the substrate is lower than that of horseradish peroxidase and shows a higher affinity to TMB than HRP, establishing the high peroxidase mimicking ability of Pd@ZIF-8. Furthermore, Pd@ZIF-8 exhibits an even superior performance toward H_2O_2 detection compared to the reported Pd-based catalysts. With the intrinsic peroxidase-like activity, the as-prepared Pd@ZIF-8 was coupled with oxidases, glucose oxidase (GOx), and cholesterol oxidase (ChOx) to develop a fluorescent sensing strategy to selectively detect the corresponding metabolites, glucose and cholesterol, respectively, as shown in Scheme 1. Accordingly, sensitive and selective biosensors were fabricated, with the linear ranges for glucose and cholesterol of 15−1000 and 5−1000 μM, respectively. The limit of detection was found to be as low as 0.10 μM for glucose and 0.092 μM for cholesterol. The bienzymic system was utilized to detect glucose and cholesterol in human blood serum, demonstrating its feasibility toward the determination of glucose for practical sample testing.

$$\text{glucose/cholesterol} + O_2 \xrightarrow{\text{GOx/ChOx}} \text{gluconic acid/cholest-4-en-3-one} + H_2O_2 \quad (1)$$

$$\text{TMB} + H_2O_2 + 2H^+ \xrightarrow{\text{Pd@ZIF-8}} \text{TMBDI} + 2H_2O \quad (2)$$

$$\text{thiamine} + H_2O_2 + OH^- \xrightarrow{\text{Pd@ZIF-8}} \text{thiochrome} + 3H_2O \quad (3)$$

https://doi.org/10.1021/acsanm.1c01712
ACS Appl. Nano Mater. 2021, 4, 9132−9142

2. EXPERIMENTAL SECTION

2.1. Chemicals. $Zn(NO_3)_2{\cdot}6H_2O$, 2-methylimidazole, Na_2PdCl_4, ascorbic acid (AA), TMB, *o*-phenylenediamine (OPD), 9,10-anthracenediyl-bis(methylene)dimalonic acid (ABDA), glucose oxidase from *Aspergillus niger* (GOx, >180 U/mg), cholesterol oxidase from microorganism (ChOX, >10 U/mg), and superoxide dismutase (SOD, >1400 U/mg) were bought from Aladdin Chemistry Co., Ltd. Mannitol, glucose, maltose, galactose, fructose, xylose, thiamine (TH), KCl, serine, threonine, bovine serum albumin (BSA), HOAc, NaOAc, NaOH, $NaBH_4$, Na_2CO_3, $NaHCO_3$, methanol, and 4-(2-hydroxyethyl)-1-piperazine ethanesulfonic acid (HEPES) were purchased from Sinopharm Chemicals Reagent Co. Ltd. (Shanghai, China). All the chemicals were of analytical grade and used as received without further purification. Ultrapure water (18.2 MΩ·cm) was obtained from a Thermal Smart2 water purification system (USA).

2.2. Synthesis of Pd@ZIF-8. First, ZIF-8 was prepared according to our previous method.[55,56] Typically, $Zn(NO_3)_2{\cdot}6H_2O$ and 2-methylimidazole were separately dispersed in methanol at a Zn^{2+} to 2-methylimidazole molar ratio of 1:8. After being stirred at room temperature for 2 h, the mixture was centrifuged and washed with methanol three times and then dried at 80 °C in an oven overnight to obtain ZIF-8 solid.

To synthesize Pd@ZIF-8, 10 mL of Na_2PdCl_4 solution (1 mg mL^{-1}) was added into 20 mL of ZIF-8 dispersion (7.5 mg mL^{-1}). After stirring for 1 h, the suspension was filtered and washed with ultrapure water three times to remove unabsorbed $PdCl_4^{2-}$. Then the powder ($PdCl_4^{2-}$@ZIF-8) was redispersed into 20 of mL H_2O through ultrasonication, and 3.43 mL of 1.5 mg·mL^{-1} $NaBH_4$ aqueous solution was quickly added to reduce Pd^{2+} for 2 h. The as-synthesized Pd@ZIF-8 was purified by filtration, washed with ultrapure water three times, and dried in a vacuum oven at 60 °C for 12 h.

2.3. Evaluation of Peroxidase-like Activity. To evaluate the peroxidase-like activity of Pd@ZIF-8, colorimetric sensing platform was adopted by using TMB as a peroxidase substrate in the presence of H_2O_2, and the UV−vis absorption was measured at 650 nm. Typically, 40 μL of Pd@ZIF-8 dispersion (2 mg mL^{-1}) was added to 330 μL of 0.2 M (pH 4.5) HOAc−NaOAc buffer, and then 20 μL of 10 mM TMB and 10 μL of 40 mM H_2O_2 were added to the mixture. pH-dependent activities were measured in reaction buffers (pH 3.6−6.0) at room temperature, while temperature-dependent activity was measured between 10 and 40 °C at pH 4.5 buffer. The steady-state kinetics of H_2O_2 or TMB were studied at a fixed TMB concentration of 500 μM or H_2O_2 concentration of 1 mM, respectively.

The kinetics of the Pd@ZIF-8 catalytic reaction were investigated by using time-dependent steady-state kinetic curves, which were conducted by varying the concentration of either TMB or H_2O_2 and fixing the Pd@ZIF-8 content to oxidize TMB. The initial rates (v_0) of TMB oxidation are determined by the molar absorption coefficient of TMBDI (ε_{TMBDI} = 39 000 M^{-1} cm^{-1} at 650 nm) using eqs 4 and 5.[1] The plots of v_0 against the concentration of H_2O_2 or TMB ([S]) indicate that the Pd@ZIF-8 catalytic reaction exhibits a typical Michaelis−Menten enzyme behavior (eq 6, Figures S5a and S5b). The K_m and maximum velocities (v_{max}) for H_2O_2 and TMB are obtained from the intercepts and slopes of the Lineweaver−Burk double-reciprocal plots which are obtained based on eqs 7 and 8 (Figures S5c and S5d).

$$[\mathrm{TMBDI}] = \frac{A}{\varepsilon_{\mathrm{TMBDI}} \times b} \tag{4}$$

$$v_0 = \frac{\Delta[\mathrm{TMBDI}]}{\Delta t} \tag{5}$$

$$\frac{1}{v_0} = \frac{K_m}{v_{max}[\mathrm{S}]} + \frac{1}{v_{max}} \tag{6}$$

$$\frac{1}{v_0} = 5.06 \times 10^7 \frac{1}{[\mathrm{H_2O_2}]} + 3.61 \times 10^6 \tag{7}$$

$$\frac{1}{v_0} = 4.69 \times 10^5 \frac{1}{[\mathrm{TMB}]} + 2.69 \times 10^6 \tag{8}$$

To investigate the enzymatic catalytic mechanisms, the intermediate free radicals $^1O_2$, ·OH, and $O_2^{\cdot-}$ were evaluated through UV−vis absorbance and electron spin resonance (ESR) spectroscopy. For the UV−vis absorbance testing of the free radicals, different scavengers, i.e., 100 μM AA, 100 μM ABDA, 100 μM mannitol, or 6.25×10^{-4} mM SOD, were used in the TMB + H_2O_2 + Pd@ZIF-8 system by virtue of time-dependent absorbance changes at 650 nm of TMB. For ESR experiments, 10 μL of 2,2,6,6-tetramethylpiperidine-1-oxyl (TEMPO) (or 5,5-dimethyl-1-pyrroline *N*-oxide (DMPO)) was mixed with 40 μL of 2 mg mL^{-1}Pd@ZIF-8, 10 μL of 40 mM H_2O_2, 20 μL of 10 mM TMB, and 320 μL of acetate buffer solution (0.2 M, pH 4.5).

2.4. Detection Procedures for H_2O_2, Glucose, and Cholesterol. H_2O_2 detection was performed by colorimetric and fluorescent methods. For colorimetric detection, 10 μL of H_2O_2 with different concentrations was added into 390 μL of 0.2 M pH 4.5 HOAc−NaOAc buffer containing 500 μM TMB and 200 μg mL^{-1} Pd@ZIF-8. After incubation for several minutes, the UV−vis absorption spectroscopy was measured. For fluorescent detection, 10 μL of H_2O_2 with different concentrations was added into 490 μL of 0.1 M pH 10.5 Na_2CO_3−$NaHCO_3$ buffer containing 50 μM TH and 20 μg mL^{-1}Pd@ZIF-8. After the mixture was incubated at 45 °C for 20 min, the H_2O_2 concentrations were quantified by testing the fluorescence intensity of thiochrome at 440 nm with excitation at 370 nm.

Glucose or cholesterol sensing was performed through the detection of the H_2O_2 generated by the corresponding oxidases (GOx or ChOX, respectively). Typically, 5 μL of glucose or cholesterol stock solutions with different concentrations was added into 25 μL of 1 M pH 7.0 HEPES buffer solution containing 40 μg mL^{-1} GOx or ChOx, which was then incubated at 37 °C for 30 min and afterward was added into 470 μL of 0.1 M (pH 10.5) Na_2CO_3−$NaHCO_3$ buffer solution containing 50 μM TH and 20 μg mL^{-1}Pd@ZIF-8. After the mixture was incubated for another 20 min, its fluorescence intensity was measured.

The detection of limit (LOD) is valued according to eq 9:

$$\mathrm{LOD} = 3\sigma/k \tag{9}$$

where σ represents the standard deviations of the blank sample, and k represents the slopes of the linear range of the detection.[57]

The recovery of the spiked glucose or cholesterol to the serum samples was determined through a standard addition method in the solution containing human serum samples. The concentrations of the glucose and cholesterol were analyzed three times through fluorescent detection methods in the presence of a human serum sample. The recovery is defined as the ratio of the detected average concentrations of glucose to the theoretical values of the dilute solutions.

2.5. Instruments. The UV−vis and fluorescence spectra were measured by UV−vis spectrophotometer (Cary 100, Agilent, Singapore) and fluorescence spectrometer (FluoroMax-4, HORIBA Jobin Yvon, Japan), respectively. Field-emission scanning electron microscopy (FE-SEM) images were collected from an S-4800 electron microscope (Hitachi, Japan). Energy dispersive spectrometer (EDS) mappings were obtained on the field-emission SEM. Transmission electron microscopy (TEM) and high-resolution transmission electron microscopy (HR-TEM) were recorded on JEM-2100 transmission electron microscopes (JEOL, Japan). Nitrogen adsorption−desorption isotherms were collected at 77 K with an Autosorb iQ one-station adsorption instrument (Quantachrome, USA). Before the measurements, samples were degassed at 150 °C for 24 h at reduced pressure. X-ray diffraction (XRD) was performed on an Ultima IV X-ray diffractometer (Rigaku, Japan) with graphite-monochrome Cu K_α radiation. X-ray photoelectron spectroscopy (XPS) experiments were carried out on an ESCALAB Xi$^+$ system (Thermo Fisher, USA) with monochrome Al K_α X-rays. Fourier transform infrared spectra (FT-IR) were tested with a NICOLET iS10 spectrometer (Thermo Fisher, USA). Electron paramagnetic resonance (ESR) signals were recorded by using an A300 ESR

https://doi.org/10.1021/acsanm.1c01712
ACS Appl. Nano Mater. 2021, 4, 9132−9142

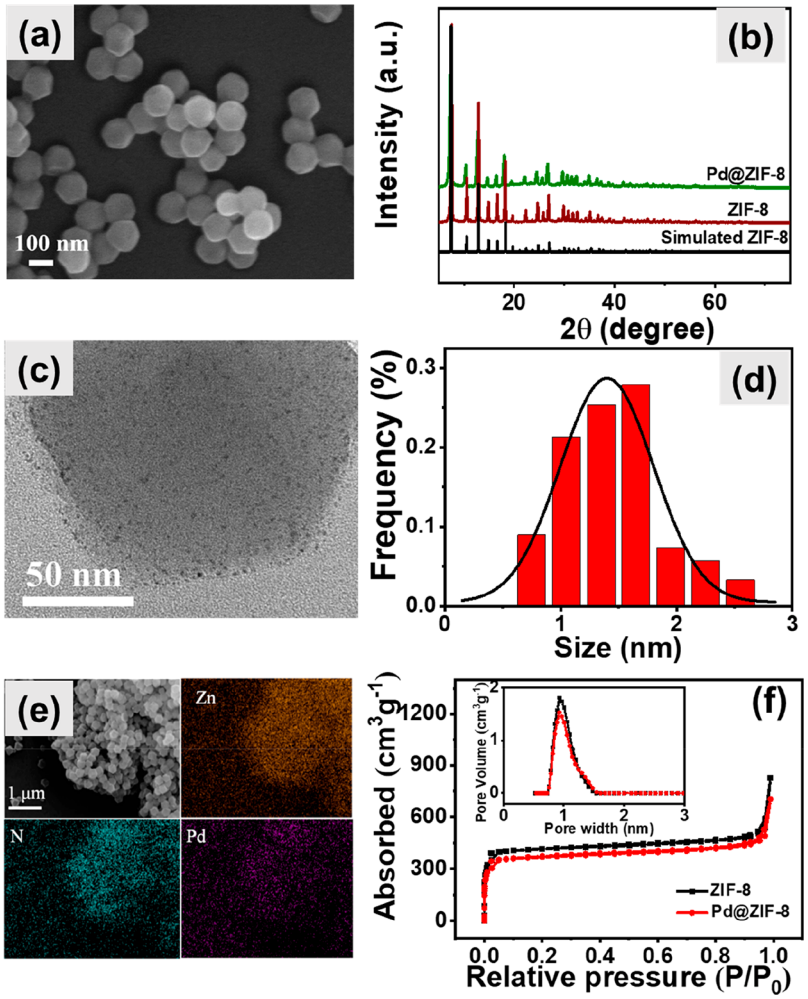

Figure 1. (a) SEM image of Pd@ZIF-8, (b) XRD patterns of simulated ZIF-8, ZIF-8, and Pd@ZIF-8, (c) TEM images of Pd@ZIF-8, (d) corresponding particle size distribution of Pd NPs in Pd@ZIF-8, (e) EDS mapping of Pd@ZIF-8, and (f) N_2 adsorption−desorption isotherms of ZIF-8 and Pd@ZIF-8. The inset shows the corresponding pore size distribution. The loading rate of Pd NPs in Pd@ZIF-8 is 0.9 atom %.

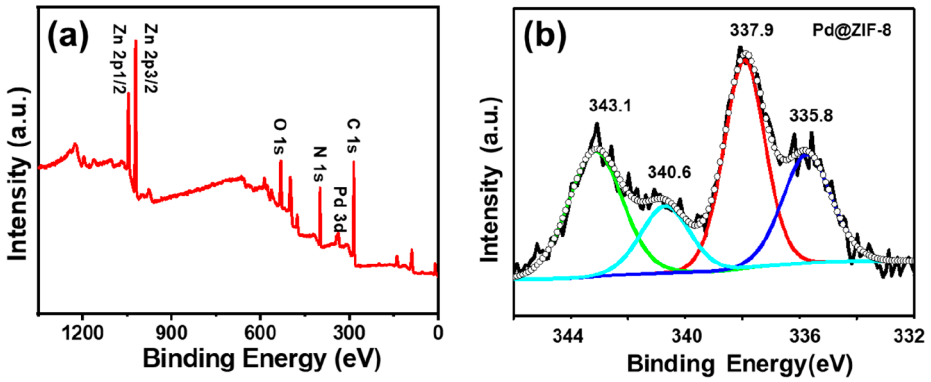

Figure 2. X-ray photoelectron (a) survey spectrum and (b) Pd 3d spectrum of Pd@ZIF-8.

spectrometer (Bruker, Germany). The Pd contents were detected by inductively coupled plasma atomic emission spectrometer (ICP-AES, Prodigy, USA).

3. RESULTS AND DISCUSSIONS

3.1. Characterization of Pd@ZIF-8. The FE-SEM images (Figure S1 and Figure 1a) show that ZIF-8 and Pd@ZIF-8 have a similar dodecahedral morphology with an average particle size of about 150 ± 20 nm, indicating that the incorporated Pd nanoclusters do not damage the topography of the ZIF-8 host. XRD patterns (Figure 1b) show that the peaks of the as-prepared ZIF-8 are identical to those of simulated ZIF-8, confirming that the high crystallinity of ZIF-8 is well maintained after hosting Pd nanoclusters. No characteristic diffraction peaks of metal Pd can be found, indicating that the metal Pd nanoclusters are highly dispersed inside ZIF-8.[58] TEM images (Figure 1c) and the corresponding particle size distribution of Pd NPs in Pd@ZIF-8 (Figure

https://doi.org/10.1021/acsanm.1c01712
ACS Appl. Nano Mater. 2021, 4, 9132−9142

1d) demonstrate that the Pd nanoclusters have a narrow distribution with an average diameter of 1.4 ± 0.6 nm. The element mappings (Figure 1e) verify that the Pd element has the same distribution as the Zn and N elements, demonstrating that Pd nanoclusters are homogeneously confined within the ZIF-8.

The effect of the Pd nanoclusters inside ZIF-8 on its pore structure and surface area was evaluated using nitrogen adsorption−desorption isotherms (Figure 1f). Based on the Brunauer−Emmett−Teller (BET) method, the surface area of Pd@ZIF-8 is calculated to be 1504 ± 2 m^2 g^{-1}, which is slightly smaller than that of ZIF-8 (1664 ± 2 m^2 g^{-1}) (Table S1).

The Barrett−Joyner−Halenda (BJH) method is employed to determine pore volume and pore size distribution. The porous volume of Pd@ZIF-8 is 0.59 ± 0.02 cm^3 g^{-1}, close to 0.62 ± 0.02 cm^3 g^{-1} for ZIF-8 (Table S1). A narrow pore size distribution of about 0.8−1.5 nm for both ZIF-8 and Pd@ZIF-8 is observed, while the pore size of Pd@ZIF-8 is slightly smaller than that of ZIF-8 (inset in Figure 1f). XPS measurements reveal that the elements C, N, Zn, and Pd with the atomic composition of 48.5%, 24.0%, 8.9%, and 0.9%, respectively, exist in Pd@ZIF-8 (Figure 2a and Table S2). The high-resolution Pd 3d XPS region of Pd@ZIF-8 is split into doublet peaks due to the spin−orbit coupling effect, which correspond to Pd $3d_{5/2}$ and Pd $3d_{3/2}$ (Figure 2b). The deconvoluted peak of Pd $3d_{5/2}$ at 335.8 eV is assigned to zero-valence palladium (Pd^0), which is about 0.7 eV higher than the standard peak value of 335.1 ± 0.1 eV for Pd^0 due to the quantum-size effect arising from the subnanometer size of the Pd nanoclusters.[59,60]

The Pd $3d_{5/2}$ deconvoluted peak with a higher binding energy at 337.9 eV is attributed to the partial ionization of the Pd surface, resulting from electron transfer from the Pd 4d to N 2p orbital, which indicates that there is strong chemical interaction between the Pd nanoclusters and ZIF-8 framework.[61] In addition, the high-resolution N 1s spectrum can be deconvoluted into three types of N species located at 398.8, 399.4, and 400.5 eV, which are assigned to pyridinic-N, Pd−N, and pyrrolic-N, respectively (Figure S2). The existence of Pd−N confirms that the metal nanoclusters are firmly anchored on ZIF-8.[62] All these results demonstrate that the high-dispersion subnanometer Pd nanoclusters were successfully prepared and chemically bonded to the ZIF-8 framework.

3.2. Peroxidase-Mimic Activity of Pd@ZIF-8. The peroxidase-mimic activity of Pd@ZIF-8 was investigated by using TMB as a chromogenic substrate in the presence of H_2O_2. When TMB, H_2O_2, and Pd@ZIF-8 coexist, the colorless TMB is converted into blue. The blue solution displays a maximum absorption at 370 and 650 nm (Figure 3), which can be attributed to the product of TMB oxidation (TMBDI). In contrast, in the absence of the Pd@ZIF-8 or when Pd@ZIF-8 replaced with ZIF-8, no obvious absorption can be seen in the TMB and H_2O_2 solution, indicating the catalytic function of the Pd@ZIF-8 toward TMB oxidation in the presence of H_2O_2. This confirms that Pd@ZIF-8 possesses a similar catalytic behavior to natural horseradish peroxidase to catalyze the decomposition of H_2O_2 substrate into hydroxyl radicals, which can oxidize the colorless TMB into blue TMBDI. Furthermore, when Pd@ZIF-8 is immersed in oxygen-saturated TMB solution in the absence of H_2O_2, the relatively weak absorbance at 370 and 650 nm can be observed. Therefore, the Pd@ZIF-8 can catalyze TMB oxidation by either H_2O_2 or dissolved O_2 and behaves as dual enzymes (oxidase and peroxidase).

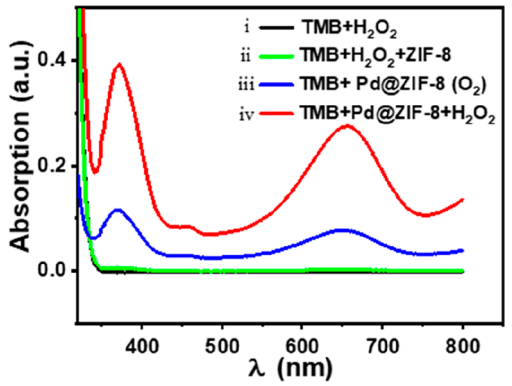

Figure 3. UV−vis spectra of TMB in different reaction systems after incubating for 10 min. The concentrations of TMB, H_2O_2, and Pd@ZIF-8 are 500 μM, 1 mM, and 200 μg mL^{-1} in the corresponding reaction system, and the total volume is 400 μL.

The peroxidase-like activity of Pd@ZIF-8 is dependent on the pH, temperature, and concentration of substrates (Figure S3). When the pH of the reaction solution is in the range of 4.0−4.5, the UV−vis adsorption of the system reaches a maximum value. This is in an agreement with Pt-based and other metal nanoenzymes; thus, pH 4.5 is chosen for all other experiments.[9,63,64] The UV−vis adsorption varies slightly with the temperature in the range of 10−40 °C; thus, the temperature influence can be ignored, and room temperature is chosen. With the increase of the H_2O_2 concentration, the UV−vis adsorption increases and reaches a plateau at 8 mM concentration. When the TMB concentration in buffer solution increases while the other conditions are kept constant, a maximum adsorption is obtained at 500 μM. Similarly, the UV−vis adsorption increases gradually with the increase of the used Pd@ZIF-8 catalysts and attains a plateau starting at 200 μg mL^{-1} (Figure S4). Therefore, the optimum conditions for the catalytic activity of Pd@ZIF-8 are pH 4.5, room temperature, and H_2O_2, TMB, and Pd@ZIF-8 concentrations of 8 mM, 500 μM, and 200 μg mL^{-1}, respectively.

To evaluate the kinetics of the Pd@ZIF-8 catalytic reaction, the K_m value was calculated according to eqs 4−8. As shown in Figure S6 and Table 1, the K_m value of 14 mM for Pd@ZIF-8 toward H_2O_2 is much lower than those of other reported noble metal based nanozymes, and the K_m value of 0.13 mM toward TMB is even lower than that of the HRP enzyme, showing a high peroxidase-like activity of Pd@ZIF-8. The high peroxidase-like activity of Pd@ZIF-8 might be attributed to the high monodispersity and numerous active catalytic sites of Pd nanoclusters and the substrate accumulation effect of the ZIF-8 supporter.

3.3. Mechanism of the Peroxidase-like Activity of Pd@ZIF-8. Previous reports illustrated that the peroxidase-like reaction of metal nanozyme proceeds as either the Fenton-like process or the electron transfer process.[69] The Fenton-like process involves the generation of reactive oxygen species during the H_2O_2 decomposition process. To verify the ROS intermediates of the Pd@ZIF-8 catalytic reaction, ascorbic acid, which can neutralize free radicals, is employed as a scavenger. It is found that the UV−vis absorbance of AA at 250 nm decreases dramatically within 10 min in the Pd@ZIF-8 + H_2O_2 + AA system due to the oxidization of AA by ROS,

https://doi.org/10.1021/acsanm.1c01712
ACS Appl. Nano Mater. 2021, 4, 9132−9142

Table 1. Comparison of K_m and v_{max} for Different Peroxidase Mimics

enzyme mimics	K_m (TMB) (mM)	K_m (H_2O_2) (mM)	v_{max} (TMB) (10^{-8} M s^{-1})	v_{max} (H_2O_2) (10^{-8} M s^{-1})	ref
Pd@ZIF-8	0.13	14.02	30.74	27.70	this work
HRP	0.52	2.53	20.37	50.48	this work
citrate−Pt NPs	0.12	205.6	6.51	9.79	19
cyt c−Pd@ZIF-8	−	6.5	−	15.19	29
Pd−Ir cubes	0.13	340	6.5	5.1	65
GK−Pd NPs	0.20	23	300	490	65
Pd/carbon dots	0.74	10.12	−	−	66
Pd nanostructures	0.16	1064	201	443	67
carboxylated chitosan-coated Pd NPs	0.09	537.71	17.7	11.2	68

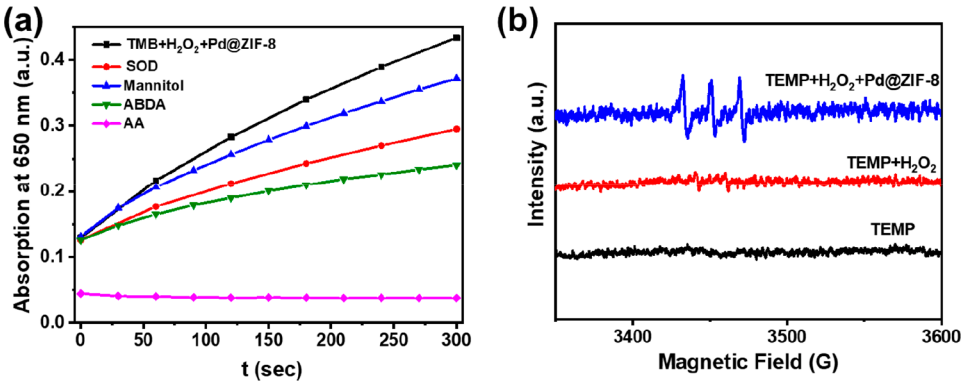

Figure 4. (a) Effects of different ROS scavengers on the kinetics of TMB oxidation based on the TMB + H_2O_2 + Pd@ZIF-8 reaction system in a total volume of 400 μL (500 μM TMB, 8 mM H_2O_2, and 200 μg mL^{-1} Pd@ZIF-8), with 1 mM AA, 1 mM ABDA, 6.25 × 10^{-3} mM SOD, or 1 mM mannitol, respectively. (b) ESR spectra demonstrating $^1O_2$ generated by Pd@ZIF-8 and H_2O_2.

which are generated in the process of Pd@ZIF-8 catalyzing H_2O_2 (Figure S7). Then, the ROS types were identified by adding scavengers, such as ABDA, SOD, or mannitol, into the Pd@ZIF-8 + TMB + H_2O_2 system. The time-dependent absorbance of TMB at 650 nm shows that in the presence of mannitol, ABDA, or SOD, the absorbance of the systems at 300 s is 0.37, 0.24 and 0.29, respectively, lower than that of the system without scavengers, which is 0.43, indicating the formation of ·OH, $^1O_2$, and $O_2^{\cdot-}$ species during the Pd@ZIF-8 catalytic process (Figure 4a).[70] This is consistent with the ROS generated by HRP (Figure S8), and the generation of ·OH, $^1O_2$, and $O_2^{\cdot-}$ affirms that Pd@ZIF-8 exhibits a Fenton-like reaction, which is further confirmed by the ESR measurements (Figure 4b and Figure S9).

3.4. H_2O_2, Glucose, and Cholesterol Sensing Based on Pd@ZIF-8. The sensing ability of Pd@ZIF-8 to H_2O_2 was explored. Since the UV−vis adsorption of the TMB + H_2O_2 + Pd@ZIF-8 reaction system is dependent on the H_2O_2 concentration, the quantitative measurement of H_2O_2 can be realized. The UV−vis absorbance of the TMB + H_2O_2 + Pd@ZIF-8 system increases with H_2O_2 concentration in a linear range from 25 to 750 μM and a relatively low detection limit of 2 μM (Figure S10). In addition, the fluorescence detection of H_2O_2 was established by using TH as a fluorescent probe, which can be oxidized by the ROS produced during the Fenton-like reaction of H_2O_2. Control experiments show that a strong emission of thiochrome (the oxidation product of TH) at 440 nm is observed, while only weak fluorescence is obtained with the TH substrate alone, Pd@ZIF-8 + TH, or TH + H_2O_2, confirming the feasibility of fluorescence detection for H_2O_2 (Figure 5). The optimum conditions for fluorescence detection of H_2O_2 are in Na_2CO_3−$NaHCO_3$ buffer (pH 10.5) at 45 °C with a catalyst dosage of 5 ng

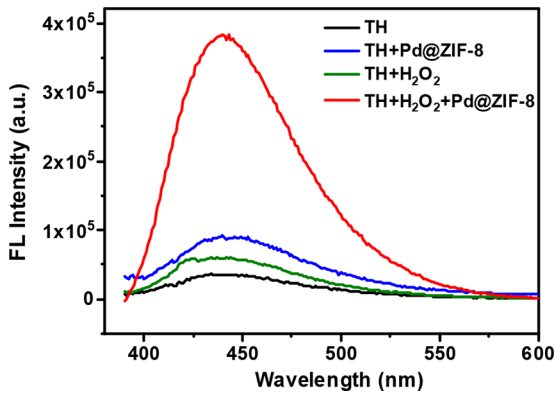

Figure 5. Fluorescence emission spectra of TH alone (black), in the presence of Pd@ZIF-8 (blue), in the presence of H_2O_2 (green), and in the presence of Pd@ZIF-8 and H_2O_2 (red).

mL^{-1} and incubation time of 20 min (Figure S11). A good linear correlation with the H_2O_2 concentration in the range of 0.5−250 μM (R^2 = 0.995) and a detection limit of 0.045 μM are obtained (Figure 6), which demonstrates an excellent performance, comparable or even superior to some reported Pd-based catalysts.[4,71,72]

The TH + H_2O_2 + Pd@ZIF-8 system with an excellent response toward H_2O_2 was set up as a universal platform for the detection of the H_2O_2 generation reaction, e.g., enzymatic catalytic glucose or cholesterol metabolism. As illustrated in reactions 1 and 3, in the presence of GOx or ChOx, glucose or cholesterol can be oxidized to gluconic acid or cholestenone and produce H_2O_2, which can be detected by TH + Pd@ZIF-8 at 440 nm. As shown in Figure 7, the fluorescence intensity at 440 nm is enhanced with the increasing concentrations of

https://doi.org/10.1021/acsanm.1c01712
ACS Appl. Nano Mater. 2021, 4, 9132−9142

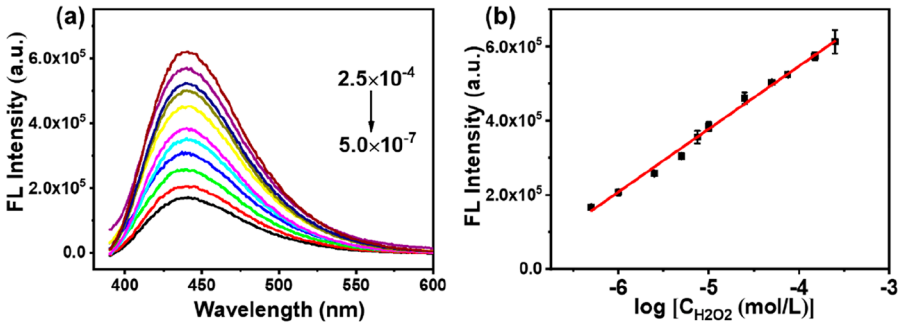

Figure 6. (a) Fluorescence spectra of TH with different concentrations of H_2O_2 in the presence Pd@ZIF-8. (b) Linear calibration plot between the fluorescence intensity at 440 nm and concentration of H_2O_2, ranging from 0.5 to 250 μM using Pd@ZIF-8 as a peroxidase mimic. Error bars represent the standard deviation for three measurements.

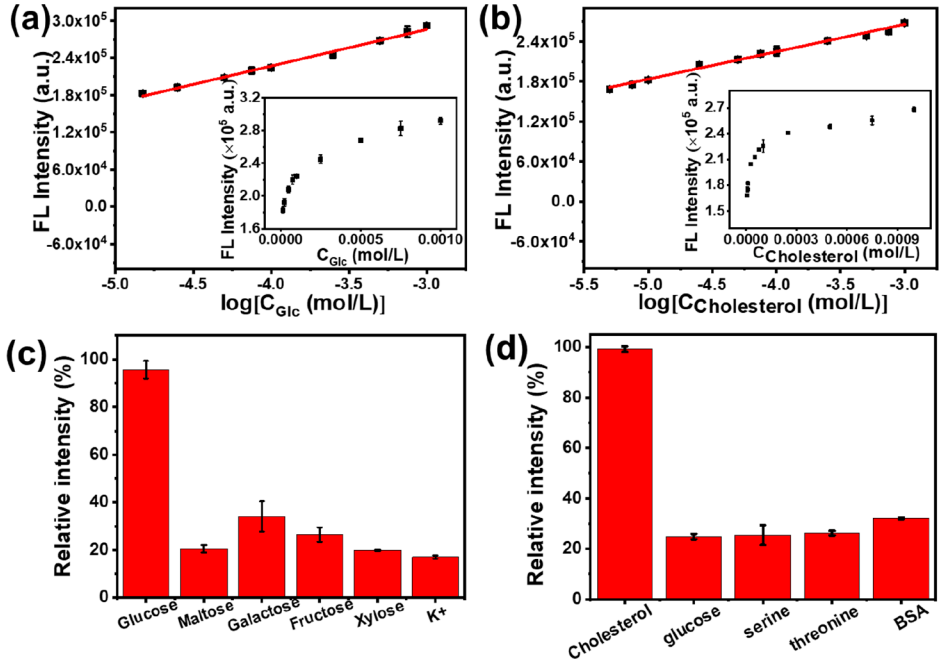

Figure 7. Linear calibration plots of the fluorescence intensity at 440 nm against the concentration of (a) glucose and (b) cholesterol. Inset: corresponding dose−response curves for glucose and cholesterol detection using Pd@ZIF-8 as a peroxidase mimic. (c) The signal difference between glucose and other interferences (maltose, galactose, fructose, xylose, and K^+), each at 1 mM. (d) The signal difference between cholesterol and other interferences (glucose, serine, threonine, and BSA), each at 1 mM. Error bars represent the standard deviation for three measurements.

glucose and cholesterol in the TH + GOx/ChOx + Pd@ZIF-8 system. For glucose detection, a linear correlation between the fluorescence intensity at 440 nm and logarithmic glucose concentration from 15 to 1000 μM and a detection limit of 1.6 μM are obtained (Figure 7a, Table 2). For cholesterol detection, the logarithmic (log) value of the cholesterol concentration and fluorescence intensity shows a good linear relationship in the concentration range from 5 to 1000 μM with a detection limit of 0.92 μM. The linear equation is defined as $FL = 3.89 \times 10^5 + 4.11 \times 10^4 \log(C_{cholesterol})$, where FL and $C_{cholesterol}$ represent the fluorescence intensity and cholesterol concentration, respectively (Figure 7b). The Pd@ZIF-8 nanozyme combined with oxidases shows a better or comparable detection limit and linear range compared to those reported nanozyme-glucose/cholesterol sensors presented in Table S2 and S3, which indicates its potential for point-of-care glucose and cholesterol monitoring.

3.5. Selectivity and Determination of Glucose and Cholesterol in Serum Samples. The selectivity of the Pd@ZIF-8-based sensor was tested by measuring glucose or cholesterol with several common interferences coexisting in

Table 2. Comparison of the Performance of Pd@ZIF-8 for Glucose Detection with Other Nanozyme-Based Glucose Biosensors

nanozymes	method	linear range (μM)	detection limit (μM)	ref
Pd@ZIF-8	fluorescent	15−1000	1.6	this work
PdNPs/g-C_3N_4	fluorescent	1−1000	0.4	4
Pd−Cu/rGO nanohybrids	colorimetric	0.5−50	0.30	73
Pt/cube-CeO_2 nanohybrids	colorimetric	0−100	4.10	74
Fe_3O_4 NPs	colorimetric	50−1000	30	75
MnO_2-modified UCNPs	fluorescent	0−250	3.7	76
CoFe-LDH/CeO_2 hybrid	colorimetric	50−2000	15	77

https://doi.org/10.1021/acsanm.1c01712
ACS Appl. Nano Mater. 2021, 4, 9132−9142

biological fluids. It is found that only glucose or cholesterol triggers a significant fluorescence signal, while other interfering substances, e.g., maltose, xylose, K^+, BSA, and serine, have negligible effect on the fluorescence response (Figure 7c and d). The excellent selectivity can be attributed to the affinity and specificity of oxidases (GOx and ChOx) toward their substrates (glucose and cholesterol, respectively).

To confirm the feasibility of the fluorescence response platform for practical applications, the fluorescent sensor was applied for detecting glucose and cholesterol in human serum samples. It is interesting to note that additionally injected glucose (or cholesterol) in the serum samples can be detected by virtue of the fluorescence response platform with a good recovery of 94.2−108.0% (Table 3), indicating the reliability of the fluorescence response platform in detecting glucose and cholesterol in human serum.

Table 3. Feasibility of the Fabricated Fluorescent Sensor in Detecting Glucose and Cholesterol in Human Serum Samples

serum sample	added (M)	found (M)	recovery (%)	RSD (%, n = 3)
glucose	1.0×10^{-4}	9.7×10^{-5}	97.1	2.23
glucose	7.5×10^{-5}	7.9×10^{-5}	105.3	1.98
glucose	5.0×10^{-5}	5.1×10^{-5}	102.4	3.63
cholesterol	1.0×10^{-4}	1.1×10^{-4}	105.0	2.33
cholesterol	7.5×10^{-5}	8.1×10^{-5}	108.0	2.50
cholesterol	5.0×10^{-5}	4.7×10^{-5}	94.2	2.37

4. CONCLUSIONS

In conclusion, the results indicate that Pd@ZIF-8 possesses intrinsic peroxidase-like activity, and its catalysis process is similar to that of horseradish peroxidase, via a Fenton-like pathway, although its product contents are slightly different. The microporous structure and abundant nitrogen sites of ZIF-8 are indispensable for the formation and immobilization of highly dispersed Pd nanoclusters. The colorimetric and fluorescent response of the Pd@ZIF-8 peroxidase-mimic is dependent on the concentration of H_2O_2, thus providing a biosensor for H_2O_2 detection. Moreover, combined with oxidases, Pd@ZIF-8 is utilized to construct a bienzyme cascade system. Through the determination of the H_2O_2 generated by the enzymatic reaction, glucose and cholesterol are successfully detected, even in human serum. Importantly, the as-prepared Pd@ZIF-8 with peroxidase-like activity exhibits several strengths over natural enzymes, such as easy synthesis, low cost, and chemical stability, which indicates that confined in MOF, nanomaterials as biomimetic catalysts can provide new opportunities for biosensor fabrication and are promising in wider applications.

■ ASSOCIATED CONTENT

Supporting Information

The Supporting Information is available free of charge at https://pubs.acs.org/doi/10.1021/acsanm.1c01712.

FE-SEM image of ZIF-8; dynamic light scattering curves of ZIF-8 and Pd@ZIF-8; N 1s XPS of Pd@ZIF-8; UV−vis for the Pd@ZIF-8 peroxidase-like activity and concentration of H_2O_2; steady-state kinetic assay of Pd@ZIF-8 and HRP; UV−vis and ESR spectra for the radicals produced during TMB oxidation; fluorescent spectra of the Pd@ZIF-8 peroxidase-like activity; the surface area and volume of micropores of materials; performance of materials for cholesterol detection (PDF)

■ AUTHOR INFORMATION

Corresponding Author

Ying Li − *Jiangsu Engineering Laboratory of Smart Carbon-Rich Materials and Device, School of Chemistry and Chemical Engineering, Southeast University, Nanjing 211189, China; Berkeley Sensor & Actuator Center and Department of Chemical and Biomolecular Engineering, University of California, Berkeley, California 94720, United States;* orcid.org/0000-0003-4875-8489; Phone: +86-25-52090613; Email: yingli@seu.edu.cn

Authors

Shujuan Li − *Jiangsu Engineering Laboratory of Smart Carbon-Rich Materials and Device, School of Chemistry and Chemical Engineering, Southeast University, Nanjing 211189, China*

Min Bao − *Jiangsu Engineering Laboratory of Smart Carbon-Rich Materials and Device, School of Chemistry and Chemical Engineering, Southeast University, Nanjing 211189, China*

Linqun Zhang − *Analytical & Testing Center, Nanjing Normal University, Nanjing 210023, China*

Carlo Carraro − *Berkeley Sensor & Actuator Center and Department of Chemical and Biomolecular Engineering, University of California, Berkeley, California 94720, United States*

Roya Maboudian − *Berkeley Sensor & Actuator Center and Department of Chemical and Biomolecular Engineering, University of California, Berkeley, California 94720, United States*

Anran Liu − *Jiangsu Engineering Laboratory of Smart Carbon-Rich Materials and Device, School of Chemistry and Chemical Engineering, Southeast University, Nanjing 211189, China;* orcid.org/0000-0002-0892-3761

Wei Wei − *Jiangsu Engineering Laboratory of Smart Carbon-Rich Materials and Device, School of Chemistry and Chemical Engineering, Southeast University, Nanjing 211189, China;* orcid.org/0000-0003-1893-1105

Yuanjian Zhang − *Jiangsu Engineering Laboratory of Smart Carbon-Rich Materials and Device, School of Chemistry and Chemical Engineering, Southeast University, Nanjing 211189, China;* orcid.org/0000-0003-2932-4159

Songqin Liu − *Jiangsu Engineering Laboratory of Smart Carbon-Rich Materials and Device, School of Chemistry and Chemical Engineering, Southeast University, Nanjing 211189, China;* orcid.org/0000-0002-4686-5291

Complete contact information is available at: https://pubs.acs.org/10.1021/acsanm.1c01712

Notes

The authors declare no competing financial interest.

■ ACKNOWLEDGMENTS

We thank the National Natural Science Foundation of China (grant nos. 21635004, 21705018, and 21775019), the USA National Science Foundation (grant no. 1903188), and the

Industrial Members of the Berkeley Sensor & Actuator Center (BSAC) for their support of this project.

REFERENCES

(1) Zhang, W.; Li, X.; Xu, X.; He, Y.; Qiu, F.; Pan, J.; Niu, X. Pd nanoparticle-decorated graphitic C_3N_4 nanosheets with bifunctional peroxidase mimicking and ON-OFF fluorescence enable naked-eye and fluorescent dual-readout sensing of glucose. *J. Mater. Chem. B* **2019**, *7*, 233−239.
(2) Song, Y.; Wei, W.; Qu, X. Colorimetric biosensing using smart materials. *Adv. Mater.* **2011**, *23*, 4215−4236.
(3) Adeniyi, O.; Sicwetsha, S.; Mashazi, P. Nanomagnet-silica nanoparticles decorated with Au@Pd for enhanced peroxidase-like activity and colorimetric glucose sensing. *ACS Appl. Mater. Interfaces* **2020**, *12*, 1973−1987.
(4) Wang, A.; Zhao, H.; Chen, X.; Tan, B.; Zhang, Y.; Quan, X. A colorimetric aptasensor for sulfadimethoxine detection based on peroxidase-like activity of graphene/nickel@palladium hybrids. *Anal. Biochem.* **2017**, *525*, 92−99.
(5) Tan, H.; Li, Q.; Zhou, Z.; Ma, C.; Song, Y.; Xu, F.; Wang, L. A sensitive fluorescent assay for thiamine based on metal-organic frameworks with intrinsic peroxidase-like activity. *Anal. Chim. Acta* **2015**, *856*, 90−95.
(6) Kotov, N. Inorganic nanoparticles as protein mimics. *Science* **2010**, *330*, 188−189.
(7) Lin, Y.; Ren, J.; Qu, X. Catalytically active nanomaterials: A promising candidate for artificial enzymes. *Acc. Chem. Res.* **2014**, *47*, 1097−1105.
(8) Liu, B.; Mosa, I.; Song, W.; Zheng, H.; Kuo, C.; Rusling, J.; Suib, S.; He, J. Unconventional structural and morphological transitions of nanosheets. *J. Mater. Chem. A* **2016**, *4*, 6447−6455.
(9) Gao, L.; Zhuang, J.; Nie, L.; Zhang, J.; Zhang, Y.; Gu, N.; Wang, T.; Feng, J.; Yang, D.; Perrett, S.; Yan, X. Intrinsic peroxidase-like activity of ferromagnetic nanoparticles. *Nat. Nanotechnol.* **2007**, *2*, 577−583.
(10) Wei, H.; Wang, E. Fe_3O_4 magnetic nanoparticles as peroxidase mimetics and their applications in H_2O_2 and glucose detection. *Anal. Chem.* **2008**, *80*, 2250−2254.
(11) Wei, H.; Wang, E. Nanomaterials with enzyme-like characteristics (nanozymes): next-generation artificial enzymes. *Chem. Soc. Rev.* **2013**, *42*, 6060−6093.
(12) Wu, J.; Wang, X.; Wang, Q.; Lou, Z.; Li, S.; Zhu, Y.; Qin, L.; Wei, H. Nanomaterials with enzyme-like characteristics (nanozymes): next-generation artificial enzymes (II). *Chem. Soc. Rev.* **2019**, *48*, 1004−1076.
(13) Dai, Z.; Guo, J.; Xu, J.; Liu, C.; Gao, Z.; Song, Y. Target-Driven Nanozyme Growth in TiO2 Nanochannels for Improving Selectivity in Electrochemical Biosensing. *Anal. Chem.* **2020**, *92* (14), 10033−10041.
(14) Miao, P.; Han, K.; Tang, Y.; Wang, B.; Lin, T.; Cheng, W. Recent advances in carbon nanodots: synthesis. *Nanoscale* **2015**, *7*, 1586−1595.
(15) Vazquez-Gonzalez, M.; Liao, W.; Cazelles, R.; Wang, S.; Yu, X.; Gutkin, V.; Willner, I. Mimicking horseradish peroxidase functions using Cu^{2+}-modified carbon nitride nanoparticles or Cu^{2+}-modified carbon dots as heterogeneous catalysts. *ACS Nano* **2017**, *11*, 3247−3253.
(16) Wang, W.; Li, Y.; Zhang, R.; He, D.; Liu, H.; Liao, S. Metal-organic framework as a host for synthesis of nanoscale Co_3O_4 as an active catalyst for CO oxidation. *Catal. Commun.* **2011**, *12*, 875−879.
(17) Sun, L.; Ding, Y.; Jiang, Y.; Liu, Q. Montmorillonite-loaded ceria nanocomposites with superior peroxidase-like activity for rapid colorimetric detection of H_2O_2. *Sens. Actuators, B* **2017**, *239*, 848−856.
(18) Jv, Y.; Li, B.; Cao, R. Positively-charged gold nanoparticles as peroxidiase mimic and their application in hydrogen peroxide and glucose detection. *Chem. Commun.* **2010**, *46*, 8017−8019.
(19) Wu, G.; He, S.; Peng, H.; Deng, H.; Liu, A.; Lin, X.; Xia, X.; Chen, W. Citrate-capped platinum nanoparticle as a smart probe for ultrasensitive mercury sensing. *Anal. Chem.* **2014**, *86*, 10955−10960.
(20) Li, J.; Liu, W.; Wu, X.; Gao, X. Mechanism of pH-switchable peroxidase and catalase-like activities of gold. *Biomaterials* **2015**, *48*, 37−44.
(21) Gutes, A.; Laboriante, I.; Carraro, C.; Maboudian, R. Palladium Nanostructures from Galvanic Displacement as a Hydrogen Peroxide Sensor. *Sens. Actuators, B* **2010**, *147*, 681−686.
(22) Jiang, H.; Chen, Z.; Cao, H.; Huang, Y. Peroxidase-like activity of chitosan stabilized silver nanoparticles for visual and colorimetric detection of glucose. *Analyst* **2012**, *137*, 5560−5564.
(23) Kim, M.; Cho, S.; Joo, S.; Lee, J.; Kwak, S.; Kim, M.; Lee, J. N- and B-doped graphene: A strong candidate to replace natural peroxidase in sensitive and selective bioassays. *ACS Nano* **2019**, *13*, 4312−4321.
(24) Li, W.; Zhi, X.; Yang, J.; Zhang, J.; Fu, Y. Colorimetric detection of cysteine and homocysteine based on an oligonucleotide-stabilized Pd nanozyme. *Anal. Methods* **2016**, *8*, 5111−5116.
(25) Chen, H.; Li, Y.; Zhang, F.; Zhang, G.; Fan, X. Graphene supported Au-Pd bimetallic nanoparticles with core-shell structures and superior peroxidase-like activities. *J. Mater. Chem.* **2011**, *21*, 17658−17661.
(26) Ge, S.; Liu, W.; Liu, H.; Liu, F.; Yu, J.; Yan, M.; Huang, J. Colorimetric detection of the flux of hydrogen peroxide released from living cells based on the high peroxidase-like catalytic performance of porous PtPd nanorods. *Biosens. Bioelectron.* **2015**, *71*, 456−462.
(27) Wei, J.; Chen, X.; Shi, S.; Mo, S.; Zheng, N. An investigation of the mimetic enzyme activity of two-dimensional Pd-based nanostructures. *Nanoscale* **2015**, *7*, 19018−19026.
(28) Jiang, D.; Ni, D.; Rosenkrans, Z.; Huang, P.; Yan, X.; Cai, W. Nanozyme: new horizons for responsive biomedical applications. *Chem. Soc. Rev.* **2019**, *48*, 3683−3704.
(29) Xia, H.; Zhong, X.; Li, Z.; Jiang, Y. Palladium-mediated hybrid biocatalysts with enhanced enzymatic catalytic performance via allosteric effects. *J. Colloid Interface Sci.* **2019**, *533*, 1−8.
(30) Lim, H.; Ju, Y.; Kim, J. Tailoring catalytic activity of Pt nanoparticles encapsulated inside dendrimers by tuning nanoparticle sizes with subnanometer accuracy for sensitive chemiluminescence-based analyses. *Anal. Chem.* **2016**, *88*, 4751−4758.
(31) Zhang, W.; Lu, G.; Cui, C.; Liu, Y.; Li, S.; Yan, W.; Xing, C.; Chi, Y.; Yang, Y.; Huo, F. A family of metal-organic frameworks exhibiting size-selective catalysis with encapsulated noble-metal nanoparticles. *Adv. Mater.* **2014**, *26*, 4056−4060.
(32) Dhakshinamoorthy, A.; Garcia, H. Catalysis by metal nanoparticles embedded on metal-organic frameworks. *Chem. Soc. Rev.* **2012**, *41*, 5262−5284.
(33) Bai, L.; Jiang, W.; Sang, M.; Liu, M.; Xuan, S.; Wang, S.; Leung, K.; Gong, X. Magnetic microspheres with polydopamine encapsulated ultra-small noble metal nanocrystals as mimetic enzymes for the colorimetric detection of H_2O_2 and glucose. *J. Mater. Chem. B* **2019**, *7*, 4568−4580.
(34) Joo, S.; Park, J.; Tsung, C.; Yamada, Y.; Yang, P.; Somorjai, G. Thermally stable Pt/mesoporous silica core-shell nanocatalysts for high-temperature reactions. *Nat. Mater.* **2009**, *8*, 126−131.
(35) Wang, Q.; Li, Y.; Liu, B.; Xu, G.; Zhang, G.; Zhao, Q.; Zhang, J. A facile reflux procedure to increase active surface sites form highly active and durable supported palladium@platinum bimetallic nanodendrites. *J. Power Sources* **2015**, *297*, 59−67.
(36) Sau, T.; Rogach, A. Nonspherical noble metal nanoparticles: colloid-chemical synthesis and morphology control. *Adv. Mater.* **2010**, *22*, 1781−1804.
(37) Astruc, D.; Lu, F.; Aranzaes, J. Nanoparticles as recyclable catalysts: The frontier between homogeneous and heterogeneous catalysis. *Angew. Chem., Int. Ed.* **2005**, *44*, 7852−7872.
(38) Chen, Z.; Cui, Z.; Niu, F.; Jiang, L.; Song, W. Pd nanoparticles in silica hollow spheres with mesoporous walls: a nanoreactor with extremely high activity. *Chem. Commun.* **2010**, *46*, 6524−6526.

https://doi.org/10.1021/acsanm.1c01712
ACS Appl. Nano Mater. 2021, 4, 9132−9142

(39) Bambagioni, V.; Bianchini, C.; Marchionni, A.; Filippi, J.; Vizza, F.; Teddy, J.; Serp, P.; Zhiani, M. Pd and Pt-Ru anode electrocatalysts supported on multi-walled carbon nanotubes and their use in passive and active direct alcohol fuel cells with an anion-exchange membrane (alcohol = methanol. *J. Power Sources* **2009**, *190*, 241−251.
(40) Guo, J.; Yang, L.; Gao, Z.; Zhao, C.; Mei, Y.; Song, Y. Insight of MOF Environment-Dependent Enzyme Activity via MOFs-in-Nano-channels Configuration. *ACS Catal.* **2020**, *10* (10), 5949−5958.
(41) Guo, J.; Yang, L.; Zhao, C.; Gao, Z.; Song, Y.; Schmuki, P. Constructing a photo-enzymatic cascade reaction and its in situ monitoring: enzymes hierarchically trapped in titania meso-porous MOFs as a new photosynthesis platform. *J. Mater. Chem. A* **2021**, *9*, 14911−14919.
(42) Huang, J.; Wang, D.; Hou, H.; You, T. Electrospun palladium nanoparticle-loaded carbon nanofibers and their electrocatalytic activities towards hydrogen peroxide and NADH. *Adv. Funct. Mater.* **2008**, *18*, 441−448.
(43) Wildgoose, G.; Banks, C.; Compton, R. Metal nanoparticles and related materials supported on carbon nanotubes: Methods and applications. *Small* **2006**, *2*, 182−193.
(44) Aijaz, A.; Karkamkar, A.; Choi, Y.; Tsumori, N.; Ronnebro, E.; Autrey, T.; Shioyama, H.; Xu, Q. Immobilizing highly catalytically active Pt nanoparticles inside the pores of metal-organic framework: A double solvents approach. *J. Am. Chem. Soc.* **2012**, *134*, 13926−13929.
(45) Gao, S.; Zhao, N.; Shu, M.; Che, S. Palladium nanoparticles supported on MOF-5: A highly active catalyst for a ligand- and copper-free Sonogashira coupling reaction. *Appl. Catal., A* **2010**, *388*, 196−201.
(46) Sabo, M.; Henschel, A.; Froede, H.; Klemm, E.; Kaskel, S. Solution infiltration of palladium into MOF-5: synthesis, physisorption and catalytic properties. *J. Mater. Chem.* **2007**, *17*, 3827−3832.
(47) Yang, Q.; Xu, Q.; Yu, S.; Jiang, H. Pd Nanocubes@ZIF-8: Integration of plasmon-driven photothermal conversion with a metal-organic framework for efficient and selective catalysis. *Angew. Chem., Int. Ed.* **2016**, *55*, 3685−3689.
(48) Azad, M.; Rostamizadeh, S.; Estiri, H.; Nouri, F. Ultra-small and highly dispersed Pd nanoparticles inside the pores of ZIF-8: Sustainable approach to waste-minimized Mizoroki-Heck cross-coupling reaction based on reusable heterogeneous catalyst. *Appl. Organomet. Chem.* **2019**, *33*, 0268−2605.
(49) Shieh, F.; Wang, S.; Yen, C.; Wu, C.; Dutta, S.; Chou, L.; Morabito, J.; Hu, P.; Hsu, M.; Wu, K.; Tsung, C. Imparting functionality to biocatalysts via embedding enzymes into nanoporous materials by a de Novo approach: Size-selective sheltering of catalase in metal-organic framework microcrystals. *J. Am. Chem. Soc.* **2015**, *137*, 4276−4279.
(50) Lyu, F.; Zhang, Y.; Zare, R.; Ge, J.; Liu, Z. One-pot synthesis of protein-embedded metal-organic frameworks with enhanced biological activities. *Nano Lett.* **2014**, *14*, 5761−5765.
(51) Ding, S.; Yan, Q.; Jiang, H.; Zhong, Z.; Chen, R.; Xing, W. Fabrication of Pd@ZIF-8 catalysts with different Pd spatial distributions and their catalytic properties. *Chem. Eng. J.* **2016**, *296*, 146−153.
(52) Jia, X.; Wang, S.; Fan, Y. A novel strategy for producing highly dispersed Pd particles on ZIF-8 through the occupation and unoccupation of carboxyl groups and its application in selective diene hydrogenation. *J. Catal.* **2015**, *327*, 54−57.
(53) Zhang, M.; Yang, Y.; Li, C.; Liu, Q.; Williams, C.; Liang, C. PVP-Pd@ZIF-8 as highly efficient and stable catalysts for selective hydrogenation of 1,4-butynediol. *Catal. Sci. Technol.* **2014**, *4*, 329−332.
(54) Zhang, T.; Li, B.; Zhang, X.; Qiu, J.; Han, W.; Yeung, K. Pd nanoparticles immobilized in a microporous/mesoporous composite ZIF-8/MSS: A multifunctional catalyst for the hydrogenation of alkenes. *Microporous Mesoporous Mater.* **2014**, *197*, 324−330.
(55) Zhu, Q.; Hu, S.; Zhang, L.; Li, Y.; Carraro, C.; Maboudian, R.; Wei, W.; Liu, A.; Zhang, Y.; Liu, S. Reconstructing hydrophobic ZIF-8 crystal into hydrophilic hierarchicallyporous nanoflowers as catalyst carrier for nonenzymatic glucose sensing. *Sens. Actuators, B* **2020**, *313*, 128031.
(56) Bao, M.; Chen, X.; Hu, S.; Zhang, L.; Li, Y.; Carraro, C.; Maboudian, R.; Wei, W.; Zhang, Y.; Liu, S. Atomically ordered intermetallic PdZn coupled with Co nanoparticles as a highly dispersed dual catalyst chemically bonded to N-doped carbon for boosting oxygen reduction reaction performance. *J. Mater. Chem. A* **2020**, *8*, 21327−21338.
(57) Wang, H.; Wang, B.; Shi, Z.; Tang, X.; Dou, W.; Han, Q.; Zhang, Y.; Liu, W. A two-photon probe for Al^{3+} in aqueous solution and its application in bioimaging. *Biosens. Bioelectron.* **2015**, *65*, 91−96.
(58) Jiang, D.; Fang, G.; Tong, Y.; Wu, X.; Wang, Y.; Hong, D.; Leng, W.; Liang, Z.; Tu, P.; Liu, L.; Xu, K.; Ni, J.; Li, X. Multifunctional Pd@UiO-66 Catalysts for Continuous Catalytic Upgrading of Ethanol to n-Butanol. *ACS Catal.* **2018**, *8*, 11973−11978.
(59) Volokitin, Y.; Sinzig, J.; deJongh, L.; Schmid, G.; Vargaftik, M.; Moiseevi, I. I. Quantum-size effects in the thermodynamic properties of metallic nanoparticles. *Nature* **1996**, *384*, 621−623.
(60) Mason, M.; Gerenser, L.; Lee, S. Electronic structure of catalytic metal clusters studied by X-ray photoemission spectroscopy. *Phys. Rev. Lett.* **1977**, *39*, 288−291.
(61) Yin, Y.; Hu, B.; Li, X.; Zhou, X.; Hong, X.; Liu, G. Pd@zeolitic imidazolate framework-8 derived PdZn alloy catalysts for efficient hydrogenation of CO_2 to methanol. *Appl. Catal., B* **2018**, *234*, 143−152.
(62) Wang, J.; Liu, W.; Luo, G.; Li, Z.; Zhao, C.; Zhang, H.; Zhu, M.; Xu, Q.; Wang, X.; Zhao, C.; Qu, Y.; Yang, Z.; Yao, T.; Li, Y.; Lin, Y.; Wu, Y.; Li, Y. Synergistic effect of well-defined dual sites boosting the oxygen reduction reaction. *Energy Environ. Sci.* **2018**, *11*, 3375−3379.
(63) Zhang, L.; Han, L.; Hu, P.; Wang, L.; Dong, S. TiO_2 nanotube arrays: intrinsic peroxidase mimetics. *Chem. Commun.* **2013**, *49*, 10480−10482.
(64) Xia, X.; Zhang, J.; Lu, N.; Kim, M.; Ghale, K.; Xu, Y.; McKenzie, E.; Liu, J.; Ye, H. Pd-Ir core-shell nanocubes: A type of highly efficient and versatile peroxidase mimic. *ACS Nano* **2015**, *9*, 9994−10004.
(65) Rastogi, L.; Karunasagar, D.; Sashidhar, R.; Giri, A. Peroxidase-like activity of gum kondagogu reduced/stabilized palladium nanoparticles and its analytical application for colorimetric detection of glucose in biological samples. *Sens. Actuators, B* **2017**, *240*, 1182−1188.
(66) Zhuo, S.; Fang, J.; Zhu, C.; Du, J. Preparation of palladium/carbon dot composites as efficient peroxidase mimics for H_2O_2 and glucose assay. *Anal. Bioanal. Chem.* **2020**, *412*, 963−972.
(67) Gao, Z.; Hou, L.; Xu, M.; Tang, D. Enhanced colorimetric immunoassay accompanying with enzyme cascade amplification strategy for ultrasensitive detection of low-abundance protein. *Sci. Rep.* **2015**, *4*, 2045−2322.
(68) He, S.; Chen, F.; Xiu, L.; Peng, H.; Deng, H.; Liu, A.; Chen, W.; Hong, G. Highly sensitive colorimetric sensor for detection of iodine ions using carboxylated chitosan-coated palladium nanozyme. *Anal. Bioanal. Chem.* **2020**, *412*, 499−506.
(69) Gao, Z.; Xu, M.; Lu, M.; Chen, G.; Tang, D. Urchin-like (gold core)@(platinum shell) nanohybrids: A highly efficient peroxidase-mimetic system for in situ amplified colorimetric immunoassay. *Biosens. Bioelectron.* **2015**, *70*, 194−201.
(70) He, F.; Mi, L.; Shen, Y.; Mori, T.; Liu, S.; Zhang, Y. Fe-N-C artificial enzyme: Activation of oxygen for dehydrogenation and monoxygenation of organic substrates under mild condition and cancer therapeutic application. *ACS Appl. Mater. Interfaces* **2018**, *10*, 35327−35333.
(71) Chen, X.; Su, B.; Cai, Z.; Chen, X.; Oyama, M. PtPd nanodendrites supported on graphene nanosheets: A peroxidase-like catalyst for colorimetric detection of H_2O_2. *Sens. Actuators, B* **2014**, *201*, 286−292.

https://doi.org/10.1021/acsanm.1c01712
ACS Appl. Nano Mater. 2021, 4, 9132−9142

(72) Chen, J.; Ge, J.; Zhang, L.; Li, Z.; Qu, L. Poly(styrene sulfonate) and Pt bifunctionalized graphene nanosheets as an artificial enzyme to construct a colorimetric chemosensor for highly sensitive glucose detection. *Sens. Actuators, B* **2016**, *233*, 438−444.
(73) Darabdhara, G.; Boruah, P.; Das, M. Colorimetric determination of glucose in solution and via the use of a paper strip by exploiting the peroxidase and oxidase mimicking activity of bimetallic Cu-Pd nanoparticles deposited on reduced graphene oxide, graphitic carbon nitride, or MoS_2 nanosheets. *Microchim. Acta* **2019**, *186*, 0026−3672.
(74) Li, Z.; Yang, X.; Yang, Y.; Tan, Y.; He, Y.; Liu, M.; Liu, X.; Yuan, Q. Peroxidase-mimicking nanozyme with enhanced activity and high stability based on metal-support interactions. *Chem. - Eur. J.* **2018**, *24*, 409−415.
(75) An, Q.; Sun, C.; Li, D.; Xu, K.; Guo, J.; Wang, C. Peroxidase-like activity of Fe_3O_4@carbon nanoparticles enhances ascorbic acid-induced oxidative stress and selective damage to PC-3 prostate cancer cells. *ACS Appl. Mater. Interfaces* **2013**, *5*, 13248−13257.
(76) Yuan, J.; Cen, Y.; Kong, X.; Wu, S.; Liu, C.; Yu, R.; Chu, X. MnO_2-nanosheet-modified upconversion nanosystem for sensitive turn-on fluorescence detection of H_2O_2 and glucose in blood. *ACS Appl. Mater. Interfaces* **2015**, *7*, 10548−10555.
(77) Yang, W.; Li, J.; Yang, J.; Liu, Y.; Xu, Z.; Sun, X.; Wang, F.; Ng, D. Biomass-derived hierarchically porous CoFe-LDH/CeO_2 hybrid with peroxidase-like activity for colorimetric sensing of H_2O_2 and glucose. *J. Alloys Compd.* **2020**, *815*, 152276.

https://doi.org/10.1021/acsanm.1c01712
ACS Appl. Nano Mater. 2021, 4, 9132−9142